How oceanic melt controls tidewater glacier evolution

Mercenier, Rémy ; Lüthi, Martin P ; Vieli, Andreas

Abstract: The recent rapid retreat of many Arctic outlet glaciers has been attributed to increased oceanic melt, but the relationship between oceanic melt and iceberg calving remains poorly understood. Here, we employ a transient finite-element model that simulates oceanic melt and ice break-off at the terminus. The response of an idealized tidewater glacier to various submarine melt rates and seasonal variations is investigated. Our modeling shows that for zero to low oceanic melt, the rate of volume loss at the front is similar or higher than for intermediate oceanic melt rates. Only very high melt rates lead to increasing volume losses. These results highlight the complex interplay between oceanic melt and calving and question the general assumption that increased submarine melt leads to higher calving fluxes and enhanced retreat. Models for tidewater glacier evolution should therefore consider calving and oceanic melt as tightly coupled processes rather than as simple, additive parametrizations.

DOI: https://doi.org/10.1029/2019gl086769

How oceanic melt controls tidewater glacier evolution

R. Mercenier[1], **M. P. Lüthi**[1], **A. Vieli**[1]

[1]Department of Geography, University of Zurich, Zurich, Switzerland

Key Points:

- The effect of oceanic melt on tidewater glacier evolution is investigated using a transient calving model based on damage evolution.
- Oceanic melt has a complex influence on tidewater glacier evolution and increased melt rates may not necessarily lead to more volume loss.
- The calving and oceanic melt processes are not additive which has implications on the forcing of models for tidewater glacier evolution.

Corresponding author: R. Mercenier, remy.mercenier@geo.uzh.ch

This article has been accepted for publication and undergone full peer review but has not been through the copyediting, typesetting, pagination and proofreading process, which may lead to differences between this version and the Version of Record. Please cite this article as doi: 10.1029/2019GL086769

Abstract

The recent rapid retreat of many Arctic outlet glaciers has been attributed to increased oceanic melt, but the relationship between oceanic melt and iceberg calving remains poorly understood. Here, we employ a transient finite-element model that simulates oceanic melt and ice break-off at the terminus. The response of an idealized tidewater glacier to various submarine melt rates and seasonal variations is investigated. Our modeling shows that for zero to low oceanic melt, the rate of volume loss at the front is similar or higher than for intermediate oceanic melt rates. Only very high melt rates lead to increasing volume losses. These results highlight the complex interplay between oceanic melt and calving and question the general assumption that increased submarine melt leads to higher calving fluxes and enhanced retreat. Models for tidewater glacier evolution should therefore consider calving and oceanic melt as tightly coupled processes rather than as simple, additive parametrizations.

1 Introduction

The current rapid retreat of ocean-terminating glaciers of the Arctic has been attributed to increased advection of warm ocean currents into the glacial fjords (e.g., Holland et al., 2008; Straneo & Heimbach, 2013; Luckman et al., 2015; Slater et al., 2018). Subaqueous melt erosion at the glacier terminus by warm water is generally assumed to result in the formation of an over-steepened calving front and therefore increased stresses and calving flux (Motyka et al., 2013; O'Leary & Christoffersen, 2013; Benn et al., 2017). This implies that increased oceanic melt drives enhanced volume loss through calving, which is also exploited in simple parametrizations of frontal ablation in models for tidewater glacier evolution (Bondzio et al., 2016; Morlighem et al., 2016; Amundson & Carroll, 2018). In a recent sophisticated modeling study, Todd et al. (2018) also demonstrated a direct influence of submarine melting on the evolution of Store Gletscher. However, their approach only allowed for a fully vertical calving front after ice break-off, and any buoyant submerged ice was removed as soon as it formed which is not fully consistent with observations (Warren et al., 1995; Motyka, 1997; Hunter & Powell, 1998; O'Neel et al., 2007; Fried et al., 2019; Sugiyama et al., 2019; Sutherland et al., 2019). The presence of submerged ice induces buoyancy forces (Warren et al., 2001; Benn et al., 2007) that alter the stresses near the calving front and consequently the calving process. Other studies have demonstrated that melt-undercutting has a limited effect on calving rates (Cook et al., 2014; Krug et al., 2015). Ma and Bassis (2019) found both an enhancing and a suppressing effect of melt on calving, depending on magnitude and vertical distribution of melt, but their simulation was limited to the onset phase of one calving event. Our own preliminary experiments with a transient Lagrangian ice-flow and damage-based calving model showed similar effects and indicated that the relationship between submarine melt and iceberg calving may not be as straightforward as previously thought (Mercenier et al., 2019). However, that study lacked a systematic investigation of the influence of oceanic melt rates on calving flux and frontal volume loss.

In this paper, we aim to better understand the link between oceanic melt, iceberg calving and volume loss for a tidewater glacier geometry that evolves over several years. We use a transient Lagrangian finite-element ice flow model that simulates ice break-off using a damage evolution law combined with the application of oceanic melt at the calving front. We investigate the response of an idealized glacier to variations of oceanic melt rate. Further, the effects of seasonality and vertical pattern in oceanic melt rate on the volume loss are evaluated.

2 Methods

We employ the transient Lagrangian multi-physics calving model developed in Mercenier et al. (2019) in two and three dimensions. This model is implemented using the libMesh finite-element library (Kirk et al., 2006). Ice flow is calculated solving the Stokes equations for incompressible fluid flow with power-law rheology (Glen's flow law). Material damage D is implemented as an evolving state variable (Pralong & Funk, 2005)

$$\frac{\partial D}{\partial t} = \max\left(B\left(\frac{\chi}{1-D} - \sigma_{\mathrm{th}}\right)^{r}, 0\right) - h\,. \tag{1}$$

that varies according to the damage rate B, a stress measure χ chosen for damage evolution, a stress threshold σ_{th}, the power r and a healing term h (for parameter settings, see Tab. S1). Damage in the ice affects its viscosity η

$$\eta = \frac{1}{2}\left(1-D\right) A^{-\frac{1}{n}} \left(\dot{\varepsilon_e} + \kappa_\varepsilon\right)^{\frac{1-n}{n}}\,. \tag{2}$$

with A the fluidity parameter, $\dot{\varepsilon_e}$ the effective strain rate, $n = 3$ the Glen's flow law exponent and κ_ε a regularization parameter. Therefore, damaged ice is softened while undamaged ice remains unaffected ($D = 0$) and a feedback between damage and the stress and velocity field is created. The model is fully Lagrangian with the state variables stored on the mesh nodes, which avoids issues with numerical diffusion as no advection problem needs to be solved. Details are given in Mercenier et al. (2019).

The model geometry is evolved over time in equal time steps calculating the velocity field and stresses. The state variable "damage" is updated according to Equation (1), and elements in contact with the ocean accumulate melt according to their interface area and oceanic melt rate. Ice removal by break-off (calving) and ocean melt is simulated with element extinction once accumulated damage exceeds a critical value or melt accumulation exceeds the element volume. The mesh nodes are subsequently moved according to nodal velocities yielding a deformed geometry. The whole domain is then horizontally moved at a constant speed u_{in}, which is chosen for each experiment to compensate average ice loss and to obtain a quasi-stationary calving front position. This horizontal movement does not influence the shape or volume loss of the modeled glaciers. The gap created at the upstream boundary by the horizontal movement is filled with new undeformed elements with their state variables set to zero. Details are given in Mercenier et al. (2019).

The damage evolution law (Eq. 1) was tested with different types of stress measure (Mercenier et al., 2019, Eq. 8). Damage evolves when the stress measure exceeds a threshold σ_{th}, leading to ice weakening and ultimately failure. From all tested stress measures, only the "von Mises" and "von Mises tensile" stress measures produced realistic calving front geometries and significant calving activity (Mercenier et al., 2019). The von Mises stress is thus used throughout this study.

Starting from a rectangular block geometry, all model runs evolved for 5 years with 5000 time steps of 0.001 year. The initial domain consisted of a simple geometry of 2000 m length and 200 m thickness, discretized with quadratic isoparametric Q2Q1 elements at a spatial resolution of 10 m. The relative water depth ($\omega = \frac{H_w}{H}$) for all experiments was set to 75% and the other model parameters are given in Table S1. The ice volume losses occurring through oceanic melt and calving were tracked separately to facilitate the analysis.

Different types of oceanic-melt experiments were performed by varying the oceanic melt rate magnitude, its seasonality, and its vertical pattern. Combinations of melt forcing parameters and their corresponding designations are listed in Table S2 and labeled with corresponding abbreviations. Oceanic melt was either continuously applied at a prescribed rate (denoted as C) or seasonally switched on and off (denoted as

S). The maximum melt rate M was varied between 0 and 1500 $\mathrm{m\,a^{-1}}$ in intervals of 250 $\mathrm{m\,a^{-1}}$ (denoted as Mx with x being the applied melt rate) which covers the main range of observed values from Greenland glaciers (Rignot et al., 2010; Carroll et al., 2016). The vertical pattern of oceanic melt was either set as constant with depth (C) or as linearly increasing from zero at the waterline to the prescribed melt rate at the bottom of the fjord (denoted as L), but any arbitrary oceanic melt parametrization as function of position and time can be prescribed in the coupled model. In the following, the term "melt" in general refers to submarine melt at the calving face.

3 Results

The whole suite of model experiments was performed on the same along-flow rectangular geometry that evolves by ice deformation, calving and melt for 5 years. During the first 1.5 years the terminus geometries self-adjust from the initial condition and to the imposed melt rates. Therefore, the evolution of volume loss (with units $\mathrm{m^3/m}$) for all experiments is only shown from 1.5 years to the end of the simulation (Fig. 2).

3.1 Melt characteristics

In the first set of model experiments, labeled CMC (Tab. S2), a continuous oceanic melt that is constant with depth was applied. The results of this set are shown in Movie S1 and Figures 1 and 2a.

Different shapes of the calving front (Fig. 1) and volume loss rates (relative to the "no melt" scenario M0; Fig. 2) are obtained for the imposed melt rates. The scenarios of high oceanic melt ($\mathrm{M} > 750\ \mathrm{m\,a^{-1}}$) show the development of an over-steepened calving face below the water line (Movie S1 and Fig. 1) and experience increasing volume losses with enhanced melt rates (Fig. 2a). In contrast, lower melt rate scenarios ($\mathrm{M} \leq 750\ \mathrm{m\,a^{-1}}$) result in decreasing volume losses with increasing oceanic melt rates (Fig. 2a), and an ice foot below the waterline develops near the base of the fjord that is more prominent for lower melt rates (Movie S1 and Fig. 1). For intermediate melt rates, the terminus geometry is undulating, with an overcut in the upper part and an undercut shape towards the grounding line.

Movie S2 shows the evolution of the glacier geometry that experiences seasonal variations in depth-averaged melt (labeled SMC). For the same melt rates as before, smaller absolute and relative volume loss differences are obtained than for the CMC scenarios (Fig. 2 and Fig. 3). During the melt season, the volume losses and geometries evolve similarly to the CMC scenarios, with the development of over-steepened calving faces (Fig. S1, between 2.6 and 3 years) and increased volume losses for the SMC1000 high melt scenario (Fig. 2b). In this scenario, the damage accumulated in the ice below the waterline remains mostly below the threshold for break-off (Fig. S1 between 2.6 and 3 years), and thus oceanic melt almost directly translates into additional volume loss. After switching off oceanic melt, the volume loss briefly decreases (Fig. S1 between 3 and 3.2 years, Movie S2), and the calving front adjusts to a similar shape and evolution as the "no melt" scenario M0, which exhibits a permanent large ice foot below the waterline. For lower melt rates the seasonal evolution of the front is very similar, although the undercutting during the melt phase is less pronounced and volume losses are slightly reduced.

Figure 2c displays the volume losses over time with seasonal oceanic melt that linearly increases with depth (denoted SML, Tab. S2). Similar geometries (Fig. S2 and Movie S3) and the same relationship between volume loss and oceanic melt are found as for the SMC scenarios. Compared to SMC the relative differences in volume loss

are slightly subdued and a melt rate exceeding 1250 m a^{-1} is necessary for a volume loss that is higher than the "no melt" scenario M0.

Figure 3 summarizes the key characteristic of our sensitivity experiments, namely that moderate oceanic melt reduces volume loss rates. Volume losses are higher for the "no melt" scenario M0 than for most scenarios with melt. For our choice of model parameters the minimum average volume loss is obtained for scenario CMC750, which is $\sim 17\%$ less than without melt. Only the scenarios with melt rates exceeding 1000 m a^{-1} show a higher volume loss than scenario M0.

The relative contribution of calving and oceanic melt to volume loss is displayed in Figure 4 for the SMC scenarios. For high seasonal melt rates (> 750 m a^{-1}) the volume loss during the melt season is dominated by oceanic melt, with almost negligible damage-induced calving. During the period without melt, damage evolution quickly recovers and calving thereby rapidly reaches a constant rate again. For lower seasonal melt rates the effect of reduced calving due to melting is also clearly apparent.

3.2 Sensitivity to damage rate and ice thickness

The competition between damage evolution and ice removal through oceanic melt determines the total volume loss, and hence advance or retreat of the terminus. Additional experiments were performed with a doubled damage rate parameter, which showed the same contrasting relationship of oceanic melt with glacier evolution, with a shift of the minimum of average volume loss towards higher values of melt rate (Fig. 5a).

The ice thickness also has a strong control on the volume loss. We modeled the response of glaciers with different initial ice thicknesses (150 m, 200 m and 250 m) to variations of oceanic melt. With increasing ice thickness, the minimum of the average volume loss occurs at higher melt rates (Fig. 5b). For the thicker glacier, higher melt rates (> 1500 m a^{-1}) lead to higher volume losses than the no melt scenario, similar to the other volume loss curves. Further, the geometries produced for the thicker glacier are similar to the glacier with an initial ice thickness of 200 m (Fig. S3).

4 Discussion

4.1 The effect of melt on tidewater glacier evolution

Melt-undercutting is generally assumed to lead to higher calving activity due to the formation of an over-steepened calving face below the waterline (Hanson & Hooke, 2000; O'Leary & Christoffersen, 2013; Benn et al., 2017). Our model results show that the effect of oceanic melt on the calving front geometry could lead to a complex behavior of tidewater glacier termini. This complexity seems to stem from the different calving front geometries below the waterline that result from the competing processes of damage evolution and oceanic melt. While calving through damage leads to an overcut of the entire calving face, oceanic melt undercuts the submerged part of the terminus, as outlined in Figure 1 and Movies S1, S2 and S3.

For our choice of geometrical and model parameters the lowest volume loss was found for a melt rate of 750 m a^{-1} (Fig. 3). For such a melt rate, the calving face undulates as a result of the competition between ice removal through damage and melt-undercutting. At higher melt rates the volume losses are increasingly dominated by melt, and therefore calving through damage is effectively shut down, as the ice is melted away before critical damage is reached (Fig. 4b). At lower melt rates, calving dominates the volume loss (Fig. 4a) and the calving front geometry is characterized by a subaqueous ice foot which is most pronounced for the "no melt" scenario M0. Such subaqueous feet are generated when calving loss above the waterline exceeds

the volume loss below (Benn et al., 2007), and have been observed at several calving glaciers (Warren et al., 1995; Motyka, 1997; Hunter & Powell, 1998; O'Neel et al., 2007; Sugiyama et al., 2019).

The presence of an ice foot induces buoyancy forces (Warren et al., 2001; Benn et al., 2007) and enhances stresses at the calving face and around the grounding line (clearly visible in panels M0 to CMC500 of Fig. 1). These stresses in turn lead to increased damaging and hence higher volume losses through calving (Fig. 4). In contrast, increasing oceanic melt reduces the length of the ice foot faster than it can break off through damage accumulation, thus reducing volume loss rates. These model results demonstrate that moderate melt rates reduce volume loss from the glacier terminus and imply that for low melt rates an increase in fjord temperatures would not necessarily induce enhanced volume loss and terminus retreat.

Large ice feet have rarely been described at ocean-terminating tidewater glaciers (e.g., Motyka, 1997). Only recently, observations from tidewater and freshwater glaciers during summer conditions have been published. These studies illustrate that many calving fronts exhibit ice feet, that occasionally reach lengths exceeding 100 m (Rignot et al., 2015; Fried et al., 2015; Bendtsen et al., 2017; Slater et al., 2018; Fried et al., 2019; Sutherland et al., 2019; Sugiyama et al., 2019). The shapes and extents of these documented terminus geometries show strong similarities with our model results. For oceanic melt rates typically estimated in Greenland fjords in summer, the modeled ice feet are reduced to 50 m or less (Fig. 1 and Movie S2), and the modeled undulating front shapes are consistent with observations (e.g., Kangerlussuup Sermia, Fried et al., 2015).

In the case of very high melt rates ($> 750\ \mathrm{m\,a^{-1}}$), as expected in vicinity of meltwater plumes (Sciascia et al., 2013; Fried et al., 2015; Slater et al., 2015, 2018), oceanic melt dominates volume loss (Fig. 4b). Melt-undercutting leads to the formation of over-steepened calving faces with large stresses (Fig. 1), but calving through damage only occurs above the waterline and hence the loss through calving remains limited. Importantly, the contrasting relationships robustly map onto the two cases of (i) low and distributed oceanic melt rates and (ii) high melt rates from meltwater plumes (Sciascia et al., 2013; Fried et al., 2015; Slater et al., 2015, 2018).

Under constant melt conditions, an increase in damage rate or ice thickness leads to an overall larger volume loss, with an increased contribution through ice break-off and consequently a reduced effect of oceanic melt. The transition from a volume loss reduction to an enhancement due to oceanic melt (Fig. 5) therefore also depends on the ice thickness and the time scale of damage evolution (damage rate parameter).

4.2 Model simplifications

The presented results apply for most tidewater glaciers with moderate thicknesses under 300 m, but potentially also apply to the larger and thicker tidewater glaciers. Further experiments would be required to investigate the behaviour of thicker glaciers.

In this study we aimed at distinguishing the effect of oceanic melt on volume loss alone, without the well-known strong control of bed geometry on tidewater glacier behavior. To use a more realistic geometry than our idealized block, and to validate the results with direct observations, several adaptations would be needed. Sliding of the glacier over the bedrock was implemented as a simple forward movement of the mesh nodes. Alternative implementations of basal motion use a frictional relationship that depends on the water pressure (e.g. Ryser et al., 2014). However, the sensitivity study of Mercenier et al. (2018) indicated that the effect of basal sliding on the stress regime at the calving front, and therefore the damage evolution, is limited, and the results presented here are robust in this regard.

The submarine melt profiles applied on the calving front were idealized to study a range of forcings. They therefore do not represent the exact melt rate distribution of any particular glacier (Ma & Bassis, 2019). The simple melt parametrizations are however sufficient to examine the effect of oceanic melt on tidewater glacier evolution.

Large submarine melt rates are often associated with narrow discharge outlets at the base of the terminus (Fried et al., 2015; Slater et al., 2018). While the runoff input drives the formation of localized plumes that only cover a portion of the terminus extent, fjord-wide circulations likely transport the warm water over most of the calving front (Slater et al., 2018). Our two-dimensional model results presented so far do not capture this spatial variability. To qualitatively assess three-dimensional effects of such localized high melt on the evolution of the calving front, we ran a preliminary simulation on an idealized three-dimensional glacier. The results of this preliminary experiment show the importance of localized high melt rates in plumes, which cut the front back and enhance the volume loss (for details, see Text S1).

Our three-dimensional modeling implies that increased melt in plumes may not only locally enhance volume loss, but trigger enhanced calving and retreat over the entire front, even if background melt rates remain relatively low. This three-dimensional effect (also found by Cowton et al. (2019)) is particularly important as plume melt rates increase with subglacial discharge, which in turn is directly linked to surface melt, and has the intriguing consequence that atmospheric warming increases the frontal volume loss (Straneo & Heimbach, 2013). This sensitivity to surface temperature is independent of any warming of ocean water.

5 Conclusions

Detailed model experiments have shown that oceanic melt has a more complex influence on tidewater glacier evolution than is commonly assumed. At very high oceanic melt rates, increased melt leads to increased volume losses. In contrast, at low to intermediate melt rates volume losses are almost constant or even decrease with increasing oceanic melt.

The complex interplay between ice fracturing processes and oceanic melt and its effect on the evolution of the calving front geometry is illustrated by our transient modeling results. In the scenarios with low or zero melt, the terminus geometry consists of a submerged ice foot that eventually breaks off due to buoyancy forces. Low to intermediate oceanic melt reduces the size of the ice foot, and consequently buoyancy forces, and thus stabilizes the glacier geometry. Only at very high melt rates the glacier evolution is dominated by the removal of submerged ice with a negative feedback on ice break-off, even with the presence of over-steepened calving faces.

Our model results highlight the necessity to consider iceberg calving and oceanic melt as tightly coupled processes that both influence the terminus geometry, which in turn affects the calving process. Simple parametrizations of calving with oceanic melt or temperatures do not capture the complexity of tidewater glacier evolution and neglect the inverted relationship at low oceanic melt rates. The susceptibility of the terminus to changes in local external forcings from meltwater plumes highlights the need for further investigation of three-dimensional effects. Calibration of model parameters with detailed observations will also be necessary to reproduce the evolution of real tidewater glaciers. This will, together with additional processes, such as the buttressing effect from ice mélange, help to better understand the calving mechanism and its link to the climate system.

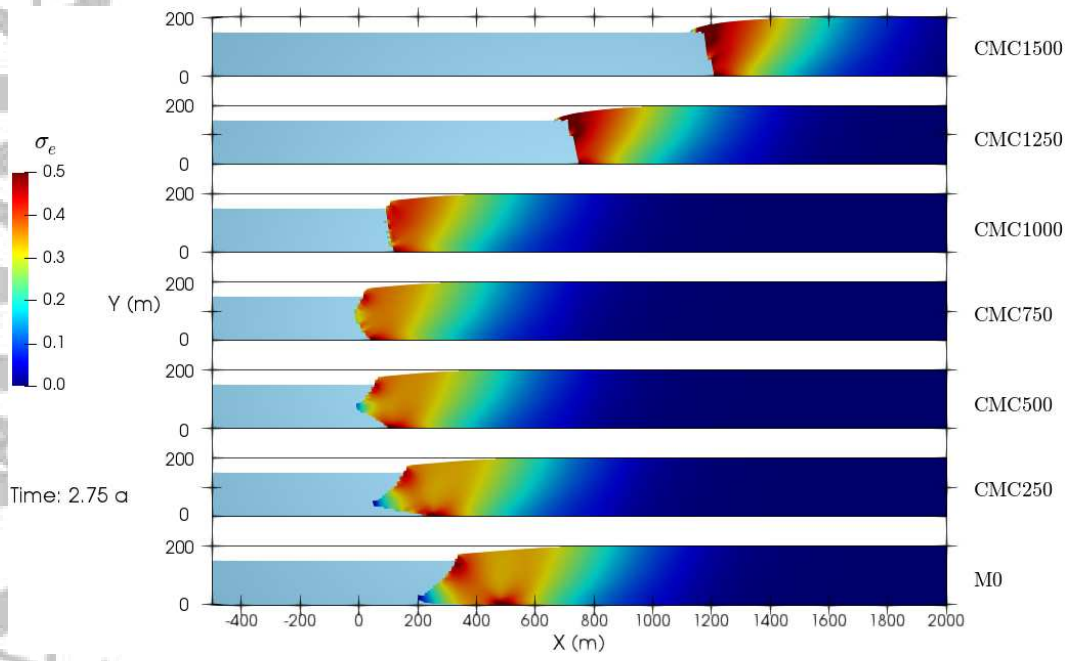

Figure 1. Von Mises stress σ_e (MPa) distribution for the continuous melt scenarios with different oceanic melt rates as labeled on the right (numbers after CMC in $\mathrm{m\,a^{-1}}$), after 2.75 years of simulation. Light blue indicates ocean water and dark lines show the bed and maximum thickness for each geometry. Note that the CMC1500 experiment is displayed with $u_{in} = 1000\,\mathrm{m}\,a^{-1}$ like all other experiments (but was run with $u_{in} = 1250\,\mathrm{m}\,a^{-1}$).

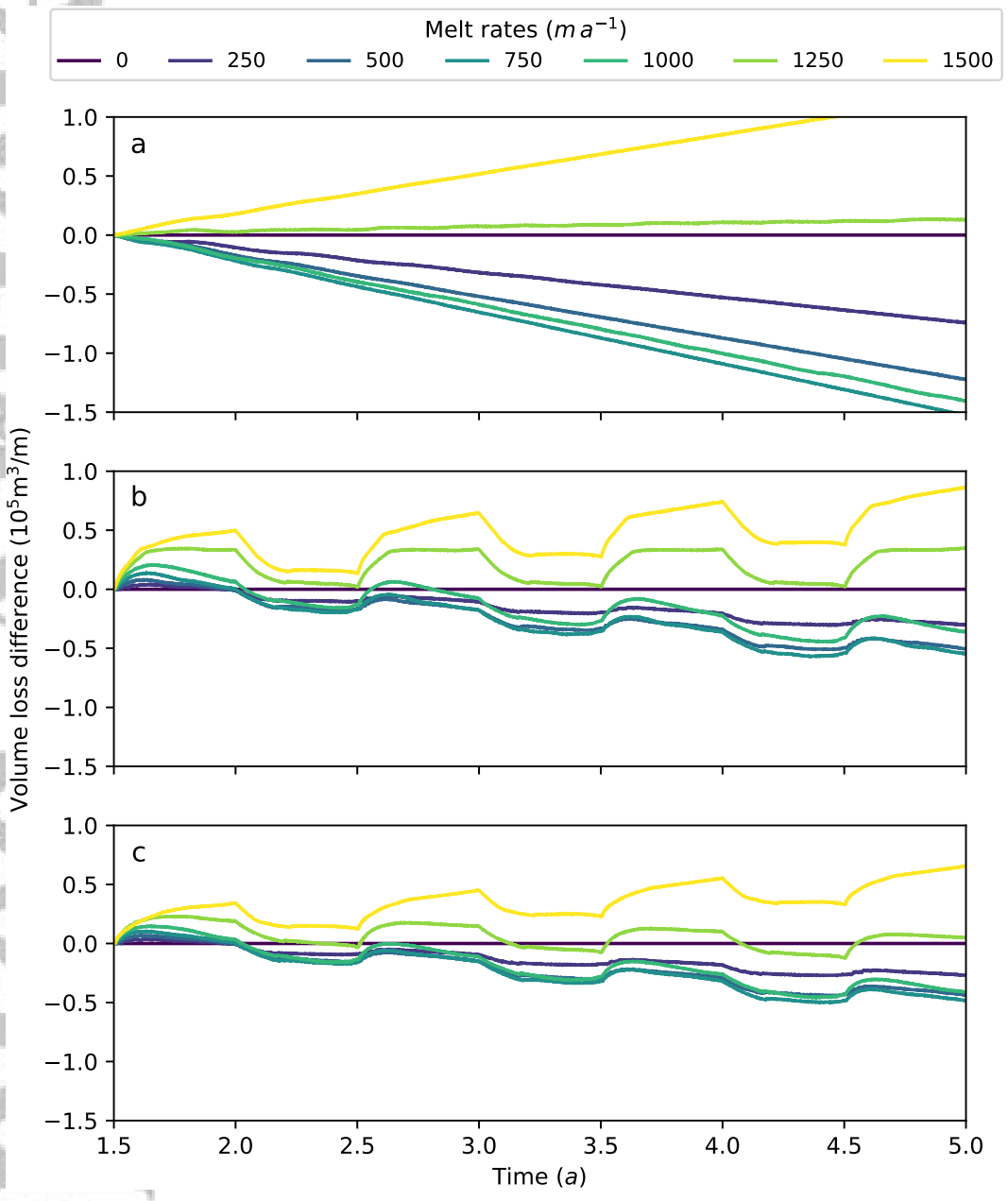

Figure 2. Cumulative volume loss difference ($10^5 m^3/m$) over time in comparison to the "no melt" scenario M0 for different melt scenarios. (a) CMC: Melt is continuous and constant with depth. (b) SMC: Melt is seasonal and constant with depth. (c) SML: Melt is seasonal and linearly increases with depth (maximum melt rate M at depth and $M = 0$ at the waterline).

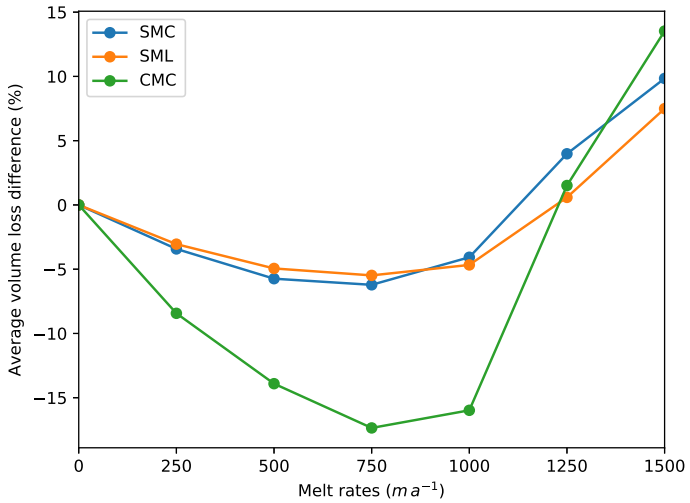

Figure 3. Average volume loss difference (%) in comparison to the "no melt" scenario M0 for the different melt scenarios.

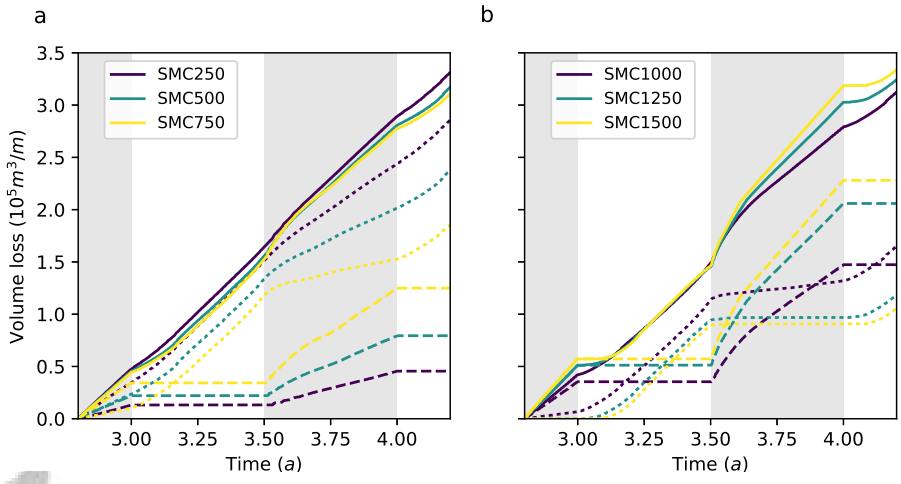

Figure 4. Cumulative volume losses for the low (a) and high (b) melt rate SMC scenarios between 2.8 and 4.2 years of simulation time. Different scenarios are represented by different colors. In addition to total volume loss (solid lines), the components of volume losses by calving (dotted lines) and oceanic melt (dashed lines) are displayed. The gray areas show the periods during which melt was applied.

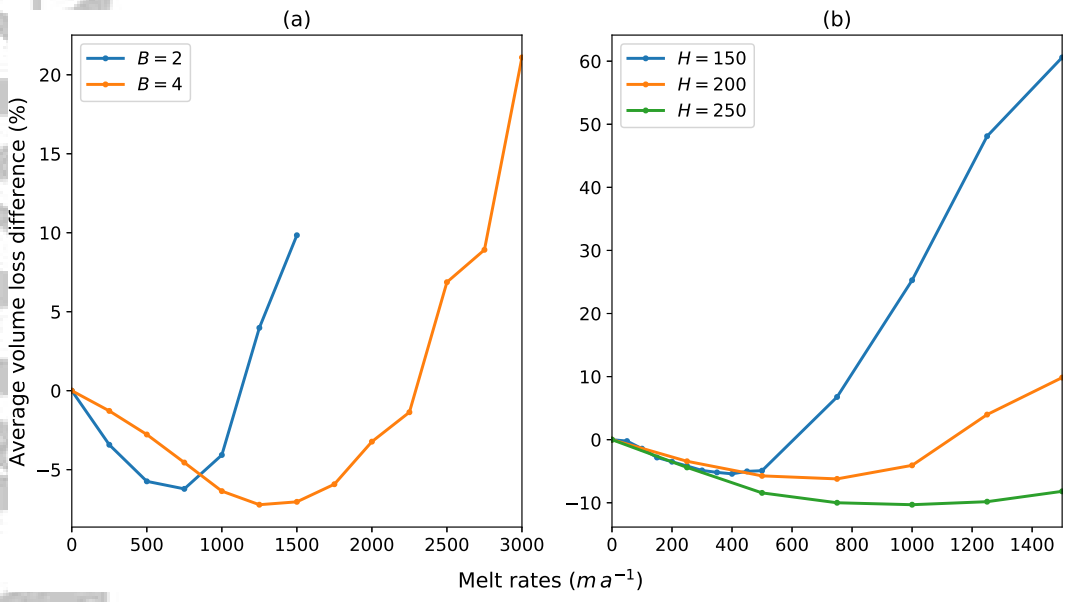

Figure 5. Average volume loss difference (%) in comparison to the "no melt" scenario M0 for different damage rates (a) and ice thicknesses (b).

Acknowledgments

The authors wish to thank the editor Mathieu Morlighem and anonymous reviewers for their comments that helped to considerably improve this paper.

The libMesh library is a C++ framework for the numerical simulation of partial differential equations on serial and parallel platforms available at `http://libmesh.github.io/` (Kirk et al., 2006). Data from this study can be obtained from `https://doi.org/10.5281/zenodo.2677937`.

This work was funded by the Swiss National Science Foundation Grant 200021-156098.

The authors declare that they have no conflict of interest.

References

Amundson, J. M., & Carroll, D. (2018, 1). Effect of topography on subglacial discharge and submarine melting during tidewater glacier retreat. *Journal of Geophysical Research: Earth Surface*. doi: 10.1002/2017JF004376

Bendtsen, J., Mortensen, J., Lennert, K., Ehn, J. K., Boone, W., Galindo, V., ... Rysgaard, S. (2017). Sea ice break up and marine melt of a retreating tidewater outlet glacier in northeast greenland (81°N). *Scientific Reports*, *7*(4941). doi: 10.1038/s41598-017-05089-3

Benn, D. I., Åström, J., Todd, J., Nick, F. M., Hulton, N. R., & Luckman, A. (2017). Melt-undercutting and buoyancy-driven calving from tidewater glaciers: new insights from discrete element and continuum model simulations. *Journal of Glaciology*, *63*(240), 691-702. doi: 10.1017/jog.2017.41

Benn, D. I., Warren, C. R., & Mottram, R. H. (2007). Calving processes and the dynamics of calving glaciers. *Earth-Science Reviews*, *82*, 143-179. doi: 10.1016/j.earscirev.2007.02.002

Bondzio, J., Seroussi, H., Morlighem, M., Kleiner, T., Rückamp, M., Humbert, A., & Larour, E. (2016). Modelling calving front dynamics using a level-set method: application to jakobshavn isbrae, west greenland. *The Cryosphere*, *10*, 497–510. doi: 10.5194/tc_10_497_2016

Carroll, D., Sutherland, D. A., Hudson, B., Moon, T., Catania, G. A., Shroyer, E. L., ... van den Broeke, M. R. (2016). The impact of glacier geometry on meltwater plume structure and submarine melt in greeland fjords. *Geophysical Research Letters*, *43*. doi: 10.1002/2016GL070170

Cook, S., Rutt, I., Murray, T., Luckman, A., Goldsack, A., & Zwinger, T. (2014). Modelling environmental influences on calving at Helheim Glacier, East Greenland. *The Cryosphere*, *7*, 4407–4442. doi: 10.5194/tc-8-827-2014

Cowton, T. R., Todd, J. A., & Benn, D. I. (2019). Sensitivity of tidewater glaciers to submarine melting governed by plume locations. *Geophysical Research Letters*, *46*. doi: 10.1029/2019GL084215

Fried, M., Catania, G., Bartholomaus, T., Duncan, D., Davis, M., Stearns, L., ... Sutherland, D. (2015). Distributed subglacial discharge drives significant submarine melt at a Greenland tidewater glacier. *Geophysical Research Letters*, *42*. doi: 10.1002/2015GL065806

Fried, M., D. Carroll, G. C., Sutherland, D. A., Stearns, L. A., Shroyer, E., & Nash, J. (2019). Distinct frontal ablation processes drive heterogeneous submarine terminus morphology. *Geophysical Research Letters*. doi: 10.1029/2019GL083980

Hanson, B., & Hooke, R. L. (2000). Glacier calving: a numerical model of forces in the calving-speed/water-depth relation. *Journal of Glaciology*, *46*(153), 188–196. doi: 10.3189/172756500781832792

Holland, D. M., Thomas, R. H., de Young, B., Ribergaard, M. H., & Lyberth, B. (2008). Acceleration of Jakobshavn Isbræ triggered by warm subsurface ocean waters. *Nature Geoscience*, *1*, 659 - 664. doi: 10.1038/ngeo316

Hunter, L. E., & Powell, R. D. (1998). Ice foot developement at temperate tidewater margins in Alaska. *Journal of Geophysical Research*, *25*(11), 1923–1926. doi: 10.1029/98GL01403

Kirk, B., Peterson, J. W., Stogner, R. H., & Carey, G. F. (2006). `libMesh`: A C++ Library for Parallel Adaptive Mesh Refinement/Coarsening Simulations. *Engineering with Computers*, *22*(3–4), 237–254. doi: 10.1007/s00366-006-0049-3

Krug, J., Durand, G., Gagliardini, O., & Weiss, J. (2015). Modelling the impact of submarine frontal melting and ice mélange on glacier dynamics. *The Cryosphere*, *9*, 989–1003. doi: 10.5194/tc-9-989-2015

Luckman, A., Benn, D. I., Cottier, F., Bevan, S., Nilsen, F., & Inall, M. (2015). Calving rates at tidewater glaciers vary strongly with ocean temperature. *Nat. Commun.*, *6:8566*. doi: 10.1038/ncomms9566

Ma, Y., & Bassis, J. N. (2019). The effect of submarine melting on calving from marine terminating glaciers. *J. Geophys. Res. Earth Surf.*. doi: 10.1029/2018JF004820

Mercenier, R., Lüthi, M. P., & Vieli, A. (2018). Calving relation for tidewater glaciers based on detailed stress field analysis. *The Cryosphere*, *12*(2), 721–739. doi: 10.5194/tc-12-721-2018

Mercenier, R., Lüthi, M. P., & Vieli, A. (2019). A transient coupled ice flow-damage model to simulate iceberg calving from tidewater outlet glaciers. *Journal of Advances in Modeling Earth Systems*, *11*, 3057–3072. doi: 10.1029/2018MS001567

Morlighem, M., Bondzio, J., Seroussi, H., Rignot, E., Larour, E., Humbert, A., & Rebuffi, S. (2016). Modeling of Store Gletschers calving dynam- ics, West Greenland, in response to ocean thermal forcing. *Geophysical Research Letters*, *43*, 26592666. doi: 10.1002/2016GL067695

Motyka, R. J. (1997). Deep-water calving at Le Conte, Southeast Alaska. In C. J. Van der Veen (Ed.), *Calving Glaciers: Report of a Workshop* (pp. 115–118). Byrd Polar Research Center, Ohio State University, Columbus, Ohio.

Motyka, R. J., Dryer, W. P., Amundson, J., Truffer, M., & Fahnestock, M. (2013). Rapid submarine melting driven by subglacial discharge, leconte glacier, alaska. *Geophysical Research Letters*, *40*, 1-6. doi: 10.1002/grl.51011

O'Leary, M., & Christoffersen, P. (2013). Calving of tidewater glaciers amplified by submarine frontal melting. *The Cryosphere*, *7*, 119–128. doi: 10.5194/tc-7-119-2013

O'Neel, S., Marshall, H., McNamara, D., & Pfeffer, W. (2007). Seismic detection and analysis of earthquakes at Columbia Glacier, Alaska. *Journal of Geophysical Research*, *112*(F03S23). doi: 10.1029/2006JF000595

Pralong, A., & Funk, M. (2005). Dynamic damage model of crevasse opening and application to glacier calving. *Journal of Geophysical Research*, *110*(B01309). doi: 10.1029/2004JB003104

Rignot, E., Fenty, I., Xu, Y., Cai, C., & Kemp, C. (2015). Undercutting of marine-terminating glaciers in West Greenland. *Geophysical Research Letters*, *42*, 5909-5917. doi: 10.1002/2015GL064236

Rignot, E., Koppes, M., & Velicogna, I. (2010). Rapid submarine melting of the calving faces of West Greenland glaciers. *Nature Geoscience*, *3*, 187-191. doi: 10.1038/NGEO765

Ryser, C., Lüthi, M., Andrews, L., Hoffman, M., Catania, G., Hawley, R., ... Kristensen, S. S. (2014). Sustained high basal motion of the Greenland Ice Sheet revealed by borehole deformation. *Journal of Glaciology*, *60*(222), 647–660. doi: 10.3189/2014JoG13J196

Sciascia, R., Straneo, F., Cenedese, C., & Heimbach, P. (2013). Seasonal variability of submarine melt rate and circulation in an East Greenland fjord. *Journal of Geophysical Research*, *118*, 2492-2502.

Slater, D. A., Nienow, P. W., Cowton, T. R., Goldberg, D. N., & Sole, A. J. (2015). Effect of near-terminus subglacial hydrology on tidewater glacier submarine melt rates. *Geophysical Research Letters*, *42*, 2861–2868. doi: 10.1002/2014GL062494

Slater, D. A., Straneo, F., Das, S. B., Richards, C. G., Wagner, T. J. W., & Nienow, P. W. (2018). Localized plumes drive front-wide ocean melting of a greenlandic tidewater glacier. *Geophysical Research Letters*, *45*, 12350–12358. doi: 10.1029/2018GL080763

Straneo, F., & Heimbach, P. (2013). North Atlantic warming and the retreat of Greenland's outlet glaciers. *Nature*, *504*, 36-43. doi: 10.1038/nature12854

Sugiyama, S., Minowa, M., & Schaefer, M. (2019). Underwater ice terrace observed at the front of glaciar grey, a freshwater calving glacier in patagonia. *Geophysical Research Letters*, *46*. doi: 10.1029/2018GL081441

Sutherland, D. A., Jackson, R. H., Kienholz, C., Amundson, J. M., Dryer, W. P., Duncan, D., ... Nash, J. D. (2019). Direct observations of submarine melt and subsurface geometry at a tidewater glacier. *Science*, *365*, 369-374. doi: 10.1126/science.aax3528

Todd, J., Christoffersen, P., Zwinger, T., Raback, P., Chauch, N., Benn, D., ... Hubbard, A. (2018). A Full-Stokes 3-D Calving Model Applied to a Large Greenlandic Glacier. *Journal of Geophysical Research: Earth Surface*, *123*, 410–432. doi: 10.1002/2017JF004349

Warren, C. R., Benn, D., Winchester, V., & Harrison, S. (2001). Buoyancy-driven lacustrine calving, Glaciar Nef, Chilean Patagonia. *Journal of Glaciology*, *47*(156), 135–146. doi: 10.3189/172756501781832403

Warren, C. R., Glasser, N. F., Harrison, S., Winchester, V., Kerr, A. R., & Rivera, A. (1995). Characteristics of tide–water calving Glaciar San Rafael. *Journal of Glaciology*, *41*(138), 273–288. doi: 10.3189/S0022143000016178

Figure 1.

σ_e
0.5
0.4
0.3
0.2
0.1
0.0

Time: 2.75 a

Y (m)

200
0
200
0
200
0
200
0
200
0
200
0
200
0
200
0

CMC1500
CMC1250
CMC1000
CMC750
CMC500
CMC250
M0

-400 -200 0 200 400 600 800 1000 1200 1400 1600 1800 2000

X (m)

Figure 2.

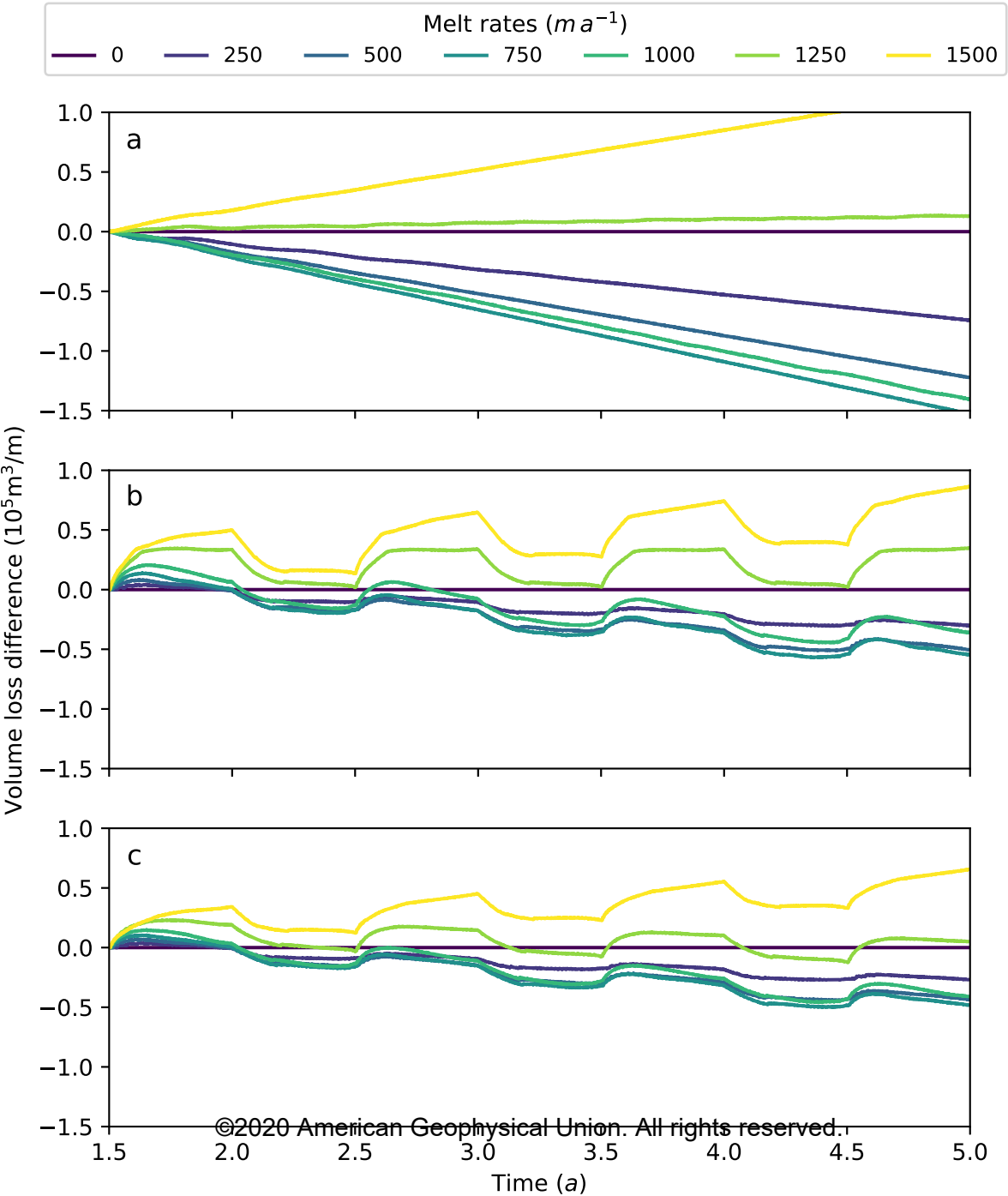

Figure 3.

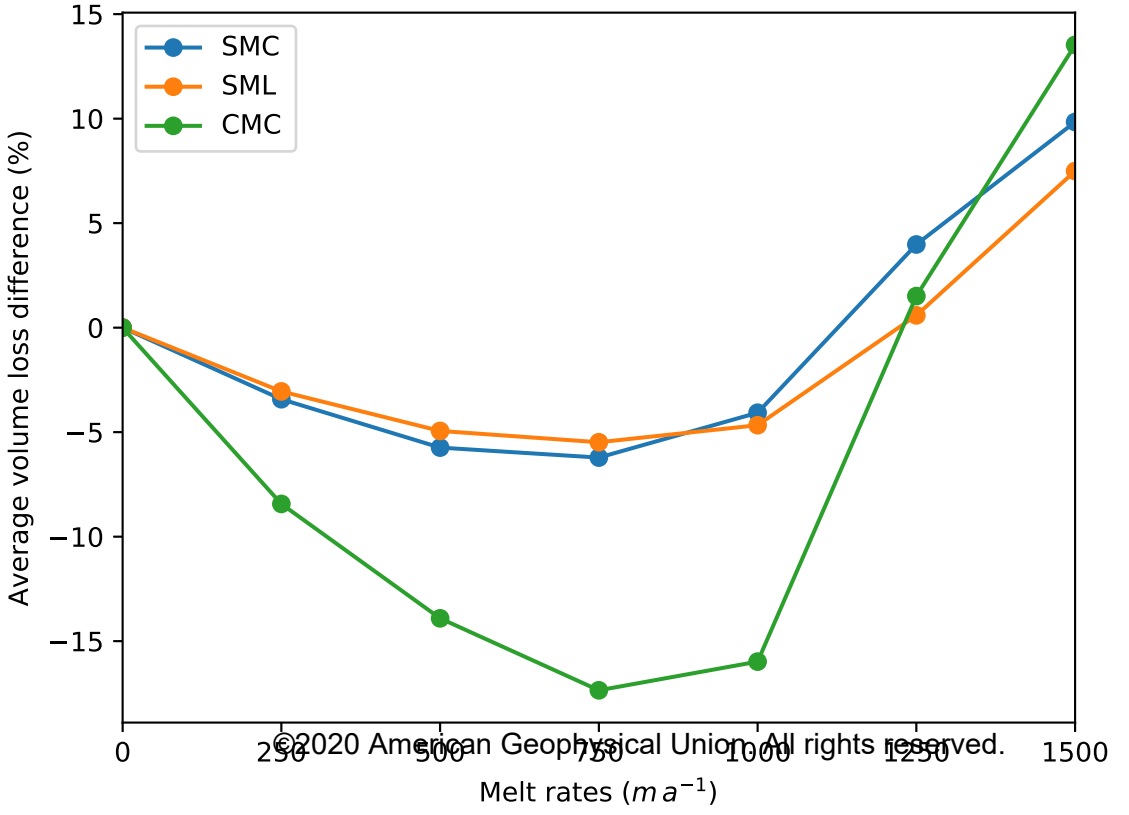

Figure 4.

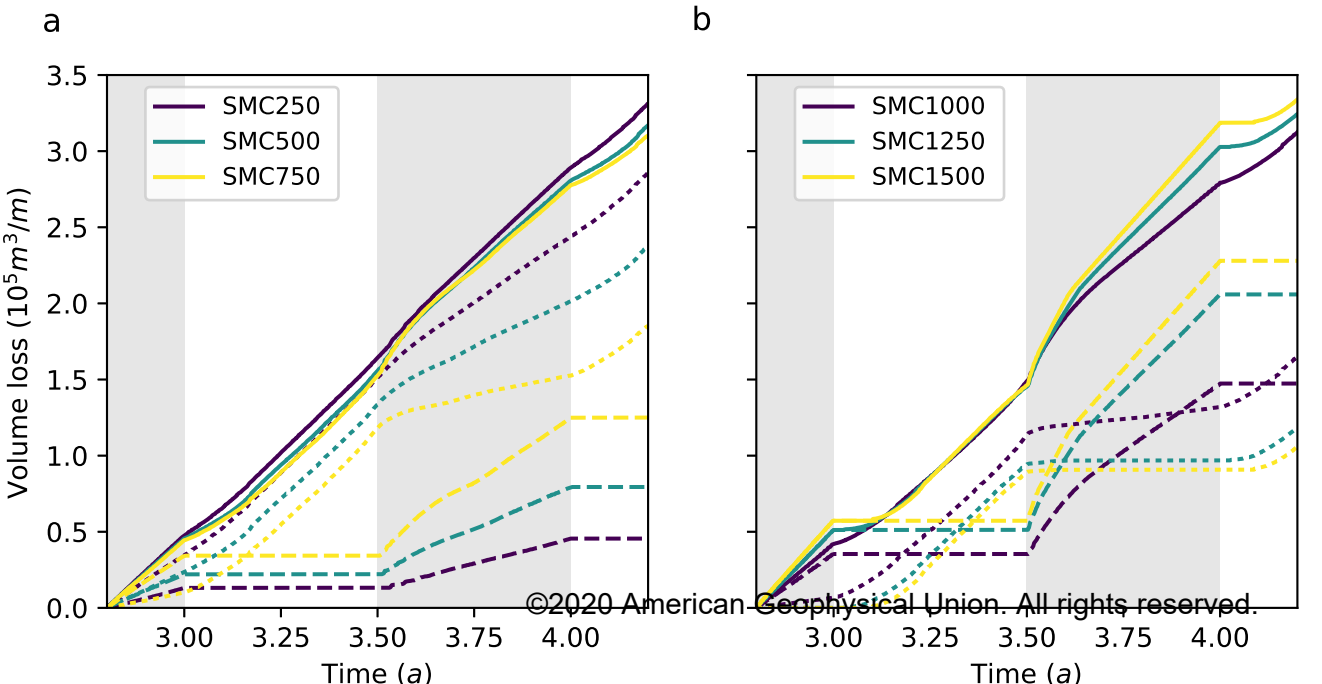

Figure 5.